Geophysical Journal International, manuscript No.
(will be inserted by the editor)

Low-frequency dispersion and attenuation in anisotropic partially saturated rocks

Short title: Seismic mesoscopic loss and anisotropy

Fabio Cavallini[1] · **José M. Carcione**[1] · **Daniel Vidal de Ventós**[2] · **Lisbeth Engell-Sørensen**[3]

Received: date / Accepted: date

Abstract The mesoscopic-loss mechanism is believed to be the most important attenuation mechanism in porous media at seismic frequencies. It is caused by P-wave conversion to slow diffusion (Biot) modes at material inhomogeneity on length scales of the order of centimeters. It is very effective in partially saturated media, particularly in the presence of gas. We explicitly extend the theory of wave propagation at normal incidence to three periodic thin layers and using this result we obtain the five complex and frequency-dependent stiffness components of the corresponding periodic finely layered medium, where the equivalent medium is anisotropic, specifically transversely isotropic. The relaxation behaviour can be described by a single complex and frequency-dependent stiffness component, since the medium consists of plane homogeneous layers.The media can be dissimilar in any property, but a relevant example in hydrocarbon exploration is the case of partial saturation and the same frame skeleton, where the fluid can be brine, oil and gas. The numerical examples illustrate the implementation of the theory to compute the wave velocities (phase and energy) and

[1]Istituto Nazionale di Oceanografia e di Geofisica Sperimentale (OGS), Borgo Grotta Gigante 42c, 34010 Sgonico, Trieste, Italy. E-mail: jcarcione@inogs.it.
[2]Lindab IMP Klima, Godovič, Slovenia.
[3]Department of Petroleum Engineering, University of Stavanger.

quality factors. We consider two main cases, namely, the same frame (or skeleton) and different fluids, and the same fluid and different frame properties. Unlike the two-phase case (two fluids), the results show two relaxation peaks. This scenario is more realistic since usually reservoirs rocks contain oil, brine and gas.

1 INTRODUCTION

An important wave-loss mechanism in porous media is wave-induced fluid flow, which occurs at different spatial scales. The flow can be classified as macroscopic, mesoscopic and microscopic. The mechanism predicted by Biot theory has a macroscopic nature (Biot, 1956). It is the wavelength-scale equilibration between the peaks and troughs of the P wave. The associated relaxation peak is located at high frequencies mainly, compared to the seismic band. Another mechanism is the local fluid flow, or "squirt" flow absorption mechanism, which has been extensively discussed in the literature (e.g., Mavko *et al.*, 2009; Carcione & Gurevich, 2011). In this mechanism, fluid-filled micro-cracks respond with greater fluid-pressure changes than the main pore space. The resulting flow at this microscopic level is the responsible for the energy loss. It has been shown that this mechanism generally does not describe the measured levels of dissipation at seismic frequencies (Diallo *et al.*, 2003).

White *et al.* (1975) have shown that attenuation and velocity dispersion measurements at the seismic band can be explained by the combined effect of mesoscopic-scale inhomogeneities and energy transfer between wave modes. We refer to this mechanism as mesoscopic loss (Pride *et al.*, 2004; Carcione & Picotti, 2006; Carcione, 2014). The mesoscopic-scale length is intended to be much larger than the grain sizes but much smaller than the wavelength of the pulse. For instance, if the fluid compressibility varies significantly from point to point, diffusion of pore fluid between different regions con-

stitutes a mechanism that can be important at seismic frequencies. White *et al.* (1975) considered two periodic dissimilar porous layers, alternately saturated with two fluids, brine and gas, specifically.

In this work, we present a generalization of the approach given in White *et al.* (1975) to the presence of N thin layers, e.g., if N =3 we may have gas, oil and brine and the same frame, which is a common situation in hydrocarbon rocks. We compute the P-wave complex modulus of a layered periodic medium in the direction perpendicular to the layering by following Norris (1993). Moreover, we extend results of Norris (1993) valid for two fluids to the case of three fluids. Then, we obtain the five stiffness components of the equivalent anisotropic medium at long wavelengths, applying the approach of Krzikalla Müller (2011) and Carcione *et al.* (2011), i.e., exploiting the 1D character of the fluid pressure equilibration process between the poroelastic layers. Because the fluid-flow direction is perpendicular to the layering plane, there is only one relaxation function, corresponding to the symmetry-axis P-wave stiffness. Therefore, knowing this relaxation function and the high- and low-frequency elastic limits of the stiffness tensor, the five complex and frequency-dependent stiffnesses of the equivalent poro-viscoelastic medium are obtained.

2 BASIC EQUATIONS FOR POROUS MEDIA

Let us consider isotropic poroelastic layers and denote the time variable by t, the frequency by f and the position vector by $\mathbf{x} = (x, y, z) = (x_1, x_2, x_3)$. Let $u^s(\mathbf{x}) = (u_1^s, u_2^s, u_3^s)$ and $u^f(\mathbf{x}) = (u_1^f, u_2^f, u_3^f)$ indicate the time Fourier transform of the displacement vector of the solid and fluid (relative to the solid) phases, respectively (if U^f is the fluid displacement vector, $u^f = \phi(U^f - u^s)$, where ϕ is the porosity). Also, set $u = (u^s, u^f)$, let $\sigma_{ij}(u)$ and $p_f(u)$ denote the time Fourier transform of the total

stress and the fluid pressure, respectively, and let $\epsilon_{ij}(u^s)$ be the strain tensor of the solid phase.

2.1 Stress-strain relation

The frequency-domain stress-strain relations of a single plane layer n in a sequence of N layers, are (Carcione 2014):

$$\sigma_{kl}(u) = 2\mu^{(n)}\,\varepsilon_{kl}(u^s) + \delta_{kl}\left(\lambda_G^{(n)}\,\nabla\cdot u^s + \alpha^{(n)}M^{(n)}\nabla\cdot u^f\right), \tag{1}$$

$$p_f(u) = -\alpha^{(n)}M^{(n)}\nabla\cdot u^s - M^{(n)}\nabla\cdot u^f. \tag{2}$$

For each layer n, the coefficient μ is the shear modulus of the bulk material, considered to be equal to the shear modulus of the dry matrix. Also

$$\lambda_G = K_G - \frac{2}{3}\mu, \tag{3}$$

with K_G the bulk modulus of the saturated material (Gassmann modulus). The coefficients in equations (1) and (2) can be obtained from the relations (Carcione 2014)

$$\alpha = 1 - \frac{K_m}{K_s}, \quad M = \left(\frac{\alpha-\phi}{K_s} + \frac{\phi}{K_f}\right)^{-1},$$

$$K_G = K_m + \alpha^2 M, \tag{4}$$

where K_s, K_m and K_f denote the bulk moduli of the solid grains, dry matrix and saturant fluid, respectively. The coefficient α is known as the effective stress coefficient of the bulk material.

2.2 Equation of motion

Let ρ_s and ρ_f denote the mass densities of the solid grains and fluid, respectively, and let

$$\rho = (1-\phi)\rho_s + \phi\rho_f \tag{5}$$

denote the mass density of the bulk material. We define the matrices

$$\mathcal{P} = \begin{pmatrix} \rho I & \rho_f I \\ \rho_f I & mI \end{pmatrix} \quad \text{and} \quad \mathcal{B} = \begin{pmatrix} 0I & 0I \\ 0I & bI \end{pmatrix}. \tag{6}$$

which are positive definite and non-negative, respectively. Here, I is the 3×3 identity matrix, the mass coupling coefficient m represents the inertial effects associated with dynamic interactions between the solid and fluid phases, while the coefficient b includes the viscous coupling effects between such phases. They are given by the relations

$$b = \frac{\eta}{\kappa}, \qquad m = \frac{\mathcal{T}\rho_f}{\phi}, \tag{7}$$

where η is the fluid viscosity, κ is the frame permeability and $\mathcal{T}$ is known as the structure or tortuosity factor. Next, let $\mathcal{L}(u)$ be the second-order differential operator defined by

$$\mathcal{L}(u) = \left[\nabla \cdot \sigma(u), -\nabla p_f(u)\right]^\top. \tag{8}$$

Then, if $\omega = 2\pi f$ is the angular frequency, Biot's equations of motion, stated in the space-frequency domain, are

$$-\omega^2 \mathcal{P} u(x,\omega) + \mathrm{i}\omega \mathcal{B} u(x,\omega) - \mathcal{L}[u(x,\omega)] = 0, \tag{9}$$

which are complemented with equations (1) and (2). We have ignored external sources in equation (9). Over the seismic band of frequencies, the inertial (acceleration) term ($-\omega^2 \mathcal{P} u(x,\omega)$) is always negligible relative to the viscous resistance and can be discarded. Therefore, at this frequency band, the effects of wave-induced fluid flow are described by the quasi-static Biot theory, i.e., stress equilibrium within the porous matrix and Darcy's flow of pore fluid. Then, the system equation to solve is the diffusion equation

$$\mathrm{i}\omega \mathcal{B} u(x,\omega) - \mathcal{L}[u(x,\omega)] = 0, \tag{10}$$

2.3 Equivalent medium

Let us consider $x_1 = x$ and $x_3 = z$ as the horizontal and vertical coordinates, respectively. As shown by Gelinsky & Shapiro (1997), the medium behaves as a TI medium with a vertical symmetry axis (the x_3-axis) at long wavelengths. They obtained the relaxed and unrelaxed limits, i.e., the low- and high-frequency limit real-valued stiffnesses, respectively. At all frequencies, the medium behaves as an equivalent (or effective) TI viscoelastic medium with complex and frequency-dependent stiffnesses, p_{IJ}, $I, J = 1, \ldots, 6$.

Denoting by τ_{ij} the stress tensor of the equivalent TI medium, the corresponding stress-strain relations, stated in the space-frequency domain, are (Carcione, 1992, 2014)

$$\tau_{11}(u) = p_{11}\ \epsilon_{11}(u^s) + p_{12}\ \epsilon_{22}(u^s) + p_{13}\ \epsilon_{33}(u^s), \tag{11}$$

$$\tau_{22}(u) = p_{12}\ \epsilon_{11}(u^s) + p_{11}\ \epsilon_{22}(u^s) + p_{13}\ \epsilon_{33}(u^s), \tag{12}$$

$$\tau_{33}(u) = p_{13}\ \epsilon_{11}(u^s) + p_{13}\ \epsilon_{22}(u^s) + p_{33}\ \epsilon_{33}(u^s), \tag{13}$$

$$\tau_{23}(u) = 2\ p_{55}\ \epsilon_{23}(u^s), \tag{14}$$

$$\tau_{13}(u) = 2\ p_{55}\ \epsilon_{13}(u^s), \tag{15}$$

$$\tau_{12}(u) = 2\ p_{66}\ \epsilon_{12}(u^s), \tag{16}$$

where we have assumed a closed system. This can be done for the undrained composite medium, for which the variation of fluid content $\zeta = -\text{div}\ u^f$ is equal to zero. This approach provides the complex velocities of the fast modes. To obtain also the complex velocity of the slow Biot wave, one needs to consider the stiffness coefficients related to the variation of fluid content and fluid pressure, where the stiffness matrix has a 7×7 dimension (Carcione 2014). The p_{IJ} are the complex and frequency-dependent Voigt

stiffnesses given in the next section. Then, we can determine the corresponding phase velocities and quality factors.

3 MESOSCOPIC-FLOW ATTENUATION THEORY FOR ANISOTROPIC POROELASTIC MEDIA

White's mesoscopic attenuation theory of interlayer flow as generalised by Norris (1993) to many dissimilar layers, based on the theory by White *et al.* (1975), describes the equivalent viscoelastic medium of a stack of thin alternating porous layers of thickness L_j, $j = 1, \ldots, N$, such that the period of the stratification is $L = \sum_j L_j$. The theory gives the complex and frequency dependent stiffness p_{33} (see Appendix A). White model has been generalized by Krzikalla & Müller (2011) to anisotropic media, i.e., they have obtained the five stiffnesses of the equivalent transversely isotropic medium as

$$p_{IJ}(\omega) = c_{IJ} + \left(\frac{c_{IJ} - c^r_{IJ}}{c_{33} - c^r_{33}} \right) [p_{33}(\omega) - c_{33}], \tag{17}$$

where c^r_{IJ} and c_{IJ} are the relaxed and unrelaxed stiffnesses, which are given in Gelinsky & Shapiro (1997) [their eqs. (14) and (15)] (see Appendix A in Carcione *et al.* (2011) and Carcione *et al.*, 2013). Using the notation of this paper those stiffnesses can be found in Carcione, (2014), equations (7.451) and (7.452), respectively.

The assumptions in Krzikalla & Müller (2011) theory are:

i) The stiffnesses matrix is symmetric (see Carcione (2014), eq. (2.24) and related discussion);

ii) The fluid-flow direction (perpendicular to layering) is independent of the loading direction and the relaxation behaviour is described by a single relaxation function or stiffness, i.e., $p_{33}(\omega)$. This means that that the theory is valid for plane layers and that a single relaxation function cannot be used in the case of 2D or 3D heterogeneities;

iii) The stiffness p_{33} used here corresponds to a periodic medium (period $= \sum_j L_j$).

The fact that the relaxed and unrelaxed shear moduli coincide implies that there is no shear loss along the directions perpendicular and parallel to layering. The qSV wave is dispersive due to its coupling with the qP wave, but the horizontally polarized SH wave is not dispersive, since $c_{55} = c_{55}^r$ and $c_{66} = c_{66}^r$ imply $p_{55} = c_{55}$ and $p_{66} = c_{66}$, according to eq (17). Moreover, an alternating sequence of thin layers saturated with different fluids but having the same shear modulus does not generate anisotropy. If there are no changes in the shear moduli, the long-wavelength equivalent Backus medium is isotropic.

Following Gelinsky Shapiro (1997), the average medium has the density

$$\bar{\rho} = \langle \rho \rangle, \tag{18}$$

where ρ is given in eq (5).

The approximate transition frequency separating the relaxed and unrelaxed states (i.e., the approximate location of the relaxation peak) is (Carcione 2014)

$$f_0 = \frac{8\kappa M E_m}{\pi \eta L^2 E_G}, \tag{19}$$

where M, $E_m = K_m + 4\mu/3$, $E_G = K_G + 4\mu/3$, η and L refer to each single layer. At this reference frequency, the Biot slow-wave attenuation length equals the mean layer thickness or characteristic length of the inhomogeneities (see next paragraph). Eq (19) indicates that the mesoscopic loss mechanism moves towards the low frequencies with increasing viscosity and decreasing permeability, i.e., the opposite behaviour of the Biot relaxation mechanism.

The mesoscopic loss mechanism is due to the presence of the Biot slow wave and the diffusivity constant is $D = \kappa M E_m/(\eta E_G)$ (Carcione, 2014). The critical fluid-diffusion relaxation length is $L_r = \sqrt{D/\omega}$. The fluid pressures will be equilibrated if

L_r is comparable to the period of the stratification. For smaller diffusion lengths (e.g., higher frequencies) the pressures will not be equilibrated, causing attenuation and velocity dispersion. Notice that the reference frequency (19) is obtained for a diffusion length $L_r = L_1/4$.

The phase and energy velocities and quality factors, which depend on frequency and propagation direction, are given in Appendix B of Carcione *et al.* (2011). The calculations using these equations requires to take the complex conjugate of p_{33} with respect to Norris (1993), since he used the opposite sign convention to define the Fourier transform.

4 EXAMPLES

We combine equations (17) and (61) to obtain the five stiffness components of a 3-layer periodic medium. Equations (64) are solved, through straightforward computations, to obtain A_j, B_j for $j = 1, 2, 3$. One obtains p_{33} (equation (61)) by substituting the values of A_j, B_j so obtained, together with (33) (d_j), (24) (R_j), (54) (a_1, b_1, a_2 and b_2), (58) (a_3 and b_3), (35) (Z_j), and (53) (C_1, S_1, C_2 and S_2).

4.1 Example 1

The first example considers the same frame and three thin layers of period $L = 60$ cm saturated with brine, oil and gas, where the properties of the rock, frame and saturant fluids are listed in Table 1. The thicknesses are $L_i = LS_i$. Figure 1 shows the phase velocity (a) and dissipation factor (b) for each case indicated in Table 2. Since the shear modulus is constant, the medium is isotropic (e.g., Berryman *et al.*, 1999; Mavko *et al.*, 2009) and because there is no P-S coupling the shear waves are lossless. Unlike the second case (where brine has the highest saturation) the other curves show two

attenuation peaks. On the basis of the transition frequency (19) the lower- and higher-frequency (mesoscopic) attenuation peaks are related to the presence of oil and gas, respectively. When both transition frequencies are similar, we can see one peak as in Case 2. For instance, the transition frequencies for Case 1 are 142 Hz (brine), 0.5 Hz (oil) and 13 Hz (gas), while those of Case 2 are 43, 1 and 37 Hz, respectively. On the other hand, as can be seen from equation (19), the peaks move to the low frequencies if the period of the layering increases.

4.2 Example 2

The next example assumes three layers of different porosity saturated with oil. The porosity affects the permeability and the dry-rock moduli as follows. Porosity and permeability are related by the Kozeny-Carman relation

$$\kappa = \frac{B\phi^3 D^2}{(1-\phi)^2} \tag{20}$$

(Mavko *et al.*, 2009), where D is the grain diameter and $B = 0.003$, where $D = 80$ μm here (sandstone).

We use the model of Krief (Mavko *et al.*, 2009) to obtain the dry-rock moduli K_m and μ_m. The porosity dependence is consistent with the concept of critical porosity, since the moduli should be small above a certain value of the porosity (usually from 0.4 to 0.6). The moduli are given by

$$\begin{aligned} K_m &= K_s(1-\phi)^{3/(1-\phi)}, \\ \mu_m &= K_m \mu_s / K_s, \end{aligned} \tag{21}$$

where K_s and μ_s are the bulk and shear moduli of the grains.

Table 3 shows the different cases, where the porosities, dry-rock moduli and permeabilities of the three layers are indicated below. Figure 2 and 3 show the phase velocity

(a) and dissipation factor (b) in the directions perpendicular and parallel to the layering, respectively. In general, there is a single relaxation peak at low frequencies (less than 0.12 Hz). The Q factors due to frame heterogeneity along the layering plane are very high and the velocity dispersion very small, as expected, since the mesoscopic loss is more significant when there is partial saturation (the preceding example). Compare also the Q factors in Figure 1 with those perpendicular to the layers in Figure 2. The polar representation of the energy velocity and dissipation factor for Case 1 is displayed in Figure 4, where the frequency is 0.06 Hz. That velocity defines the wavefront related to each frequency if multiplied by one unit of time. As can be seen, the qP wave has a stronger attenuation along the vertical direction and the qSV wave is lossless along the layering plane and vertical direction. The observed attenuation is due to the coupling with the qP wave. The SH wave is lossless since it is a pure mode, uncoupled from the other two waves. Let us replace oil with brine. Figure 5 shows the phase velocity (a) and dissipation factor (b) in the directions perpendicular to the layering. As can be appreciated, the maximum attenuation occurs at higher frequencies, due to the lower viscosity of brine, in agreement with equation (19).

4.3 Example 3

Finally, we consider the cases of Table 3, where layers 1 and 2 are saturated with oil and layer 3 with gas. The phase velocity (a) and dissipation factor (b) versus frequency perpendicular and parallel to the layering plane are presented in Figures 6 and 7, respectively. As expected, the presence of partial saturation increases drastically the attenuation and velocity dispersion in comparison with the previous example.

5 CONCLUSIONS

Mesoscopic loss is the most effective attenuation mechanism at seismic frequencies since the amount of attenuation and velocity dispersion can be related to the microstructural characteristics of the rock and its pore fill. Information, such as permeability, porosity, fluid modulus, and viscosity, may, in principle, be inferred from the amplitude and relative propagation time of the seismic pulse. The amount of loss because of partial saturation and porosity variations is more important compared to other causes, such as variations of the grain and dry-rock frame moduli. Here, we have considered three flat layers with different properties. In general, the effective medium, i.e., at long wavelengths compared to the thickness of the layers, is anisotropic in velocity and attenuation. We have explicitly solved the problem for three layers, which allows us to consider three fluids, i.e., partial saturation with oil, brine and gas for instance, a more realistic situation compared to the two-phase case considered in the literature. The equations are valid for three different frames as well.

The first example considers the same frame saturated with brine, oil and gas. Since the shear modulus is constant, the medium is isotropic and because there is no P-S coupling, the shear waves are lossless. The curves show two attenuation peaks unlike the two-fluid case. If the period of the layering increases, the peaks move to the low frequencies. A second example assumes three layers of different porosity saturated with oil. In general, there is a single relaxation peak at low frequencies. The Q factors due to frame heterogeneity along the layering plane are very high and the velocity dispersion very small, as expected, since the mesoscopic loss is more significant when there is partial saturation (the preceding example). The qP wave has a stronger attenuation along the vertical direction and the qSV wave is lossless along the layering plane and

vertical direction. The observed attenuation is due to the coupling with the qP wave. When replacing oil with brine, the maximum attenuation occurs at higher frequencies, due to the lower viscosity of brine. Finally, partial saturation increases drastically the attenuation and velocity dispersion in comparison with the previous case.

ACKNOWLEDGMENTS

One of the authors (F. C.) is grateful to Géza Seriani and Davide Gei for encouragement and advice.

REFERENCES

Berryman, J. G., Grechka, V. Y., & Berge, P., 1999. Analysis of Thomsen parameters for finely layered VTI media, *Geophys. Prospect.*, **47**, 959–978.

Biot, M. A., 1956. Theory of propagation of elastic waves in a fluid-saturated porous solid. I. Low-frequency range, *J. Acoust. Soc. Am.*, **28**, 168–178.

Carcione, J. M., 1992. Anisotropic Q and velocity dispersion of finely layered media, *Geophysical Prospecting*, **40**, 761–783.

Carcione, J. M., 2014, Wave fields in real media: Wave propagation in anisotropic, anelastic, porous and electromagnetic media, Handbook of Geophysical Exploration, Elsevier, Amsterdam (3rd edition, revised and extended).

Carcione, J. M., & Gurevich, B., 2011. Differential form and numerical implementation of Biot's poroelasticity equations with squirt dissipation, *Geophysics*, **76**, N55–N64.

Carcione, J. M., Gurevich, B., and Santos, J. E., & Picotti, S., 2013. Angular and frequency dependent wave velocity and attenuation in fractured porous media, *Pure and Applied Geophysics*, **170**,1673–1683.

Carcione, J. M., & Picotti, S., 2006. P-wave seismic attenuation by slow-wave diffusion. Effects of inhomogeneous rock properties, *Geophysics*, **71**, O1–O8.

Carcione, J. M., Santos, J. E., & Picotti, S., 2011. Anisotropic poroelasticity and wave-induced fluid flow. Harmonic finite-element simulations, *Geophys. J. Internat.*, **186**, 1245–1254.

Diallo, M. S., Prasad, M., & Appel, E., 2003. Comparison between experimental results and theoretical predictions for P-wave velocity and attenuation at ultrasonic frequency, *Wave Motion*, **37**, 1–16.

Gelinsky, S., & Shapiro, S. A., 1997. Dynamic-equivalent medium approach for thinly layered saturated sediments, *Geophys. J. Internat.*, **128**, F1–F4.

Krzikalla, F., & Müller, T., 2011. Anisotropic P-SV-wave dispersion and attenuation due to inter-layer flow in thinly layered porous rocks, *Geophysics*, **76**, WA135–WA145.

Mavko, G., Mukerji, T., & Dvorkin, J., 2009, The rock physics handbook, Cambridge Univ. Press.

Norris, A. N., 1993. Low-frequency dispersion and attenuation in partially saturated rocks, *J. Acoust. Soc. Am.*, **94**, 359–370.

Pride, S. R., Berryman, J. G., & Harris, J. M., 2004. Seismic attenuation due to wave-induced flow, *J. Geophys. Res.*, **109**, B01201, 1–19.

White, J. E., Mikhaylova, N. G., & Lyakhovitskiy, F. M., 1975. Low frequency seismic waves in fluid saturated layered rocks, *Izvestija Academy of Sciences USSR, Physics of the Solid Earth*, **11**, 654–659.

A : MESOSCOPIC-LOSS THEORY FOR MANY LAYERS

The theory to obtain p_{33} is based on Norris (1993). For brevity, we refer to his equations when necessary.

A.1 Single layer

A.1.1 Prerequisites

For convenience, eqs. (25-Norris), using our notation, are rewritten here as

$$P' = -\frac{\eta}{\kappa} W \tag{22}$$

$$W' = \frac{\mathrm{i}\,\omega\,\alpha}{K_m + \frac{4}{3}\,\mu}\,(R^{-1}\,P - 1) \tag{23}$$

where, by (26-Norris),

$$R = \frac{\alpha\,M}{K_G + \frac{4}{3}\,\mu}. \tag{24}$$

Equation (22) is the diffusion equation for the dimensionless pressure P and the prime indicates the spatial derivative with respect to spatial variable z.

Moreover, we need the diffusion coefficient given by (28-Norris), namely,

$$D = \frac{\kappa}{\eta}\,M\,\frac{K_m + \frac{4}{3}\,\mu}{K_G + \frac{4}{3}\,\mu} \tag{25}$$

A.1.2 Rearrangement of (25a-Norris)

Differentiating (22) yields

$$P'' = -\frac{\eta}{\kappa} W'$$

and hence, solving for W',

$$W' = -\frac{\kappa}{\eta} P'' \tag{26}$$

A.1.3 Rearrangement of (25b-Norris)

Dividing (25) by (24) and rearranging, we get

$$K_m + \frac{4}{3}\,\mu = \frac{D\,\alpha\,\eta}{\kappa\,R} \tag{27}$$

which, substituted into (23), yields

$$W' = \frac{\mathrm{i}\,\omega\,\kappa}{D\,\eta}\,(P - R) \tag{28}$$

A.1.4 Derivation of (A1-Norris) and (A2-Norris)

Substituting (26) into (28) and rearranging, we get

$$P'' = -\frac{\omega}{D}\,\mathrm{i}\,(P-R) \tag{29}$$

The coefficient in (29) may be rewritten as

$$\frac{\omega}{D}\,\mathrm{i} = \gamma^2 \qquad \text{with} \qquad \gamma := \exp\left(\mathrm{i}\,\frac{\pi}{4}\right)\sqrt{\frac{\omega}{D}} \tag{30}$$

so that (29) becomes

$$P'' = -\,\gamma^2\,(P-R) \tag{31}$$

Assuming that γ and R are constants, the general solution of (31) is

$$P = P_0 + R \qquad \text{with} \qquad P_0 = A\,\cos(\gamma\,z) + B\,\sin(\gamma\,z) \tag{32}$$

Equation (32) is made equivalent to the first of eqs. (A1-Norris) by defining

$$d := \ell\,\gamma \tag{33}$$

with ℓ representing the thickness of the layer, consistently with the second of eqs. (A2-Norris).

From (22) we get

$$W = -\,\frac{\kappa}{\eta}\,P'$$

and hence, using (32),

$$W = \frac{1}{Z}\left[A\,\sin(\gamma\,z) - B\,\cos(\gamma\,z)\right] \tag{34}$$

which is made equivalent to the second of eqs. (A1-Norris) by defining

$$Z := \frac{\eta}{\kappa\,\gamma} \tag{35}$$

consistently with the first of eqs. (A2-Norris).

A.2 Many layers

Substituting (32) into (24b-Norris), namely,

$$\frac{1}{p_{33}} = \left\langle \frac{1-\alpha\,P}{K_m + \frac{4}{3}\,\mu} \right\rangle \tag{36}$$

yields

$$\frac{1}{p_{33}} = \left\langle \frac{1-\alpha\,R}{K_m + \frac{4}{3}\,\mu} \right\rangle - \left\langle \frac{\alpha}{K_m + \frac{4}{3}\,\mu}\,P_0 \right\rangle \tag{37}$$

Using equation (4) and noting that

$$1-\alpha\,R \overset{(24)}{=} 1 - \frac{\alpha^2\,M}{K_G + \frac{4}{3}\,\mu} \overset{(4)}{=} \frac{K_m + \frac{4}{3}\,\mu}{K_G + \frac{4}{3}\,\mu}$$

we get

$$\frac{1-\alpha\,R}{K_m + \frac{4}{3}\,\mu} = \frac{1}{K_G + \frac{4}{3}\,\mu}$$

and hence the first term at the r.h.s. of (37) is

$$\left\langle \frac{1-\alpha\,R}{K_m+\frac{4}{3}\,\mu} \right\rangle = \left\langle \frac{1}{K_G+\frac{4}{3}\,\mu} \right\rangle \overset{\text{(13-Norris)}}{=} \frac{1}{c_{33}}$$

($c_{33} = C_\infty$ in Norris), so that (37) becomes

$$\frac{1}{p_{33}} = \frac{1}{c_{33}} - \langle \psi\, P_0 \rangle \tag{38}$$

($p_{33} = C^*$ in Norris), where, for convenience, we introduce

$$\psi := \frac{\alpha}{K_m+\frac{4}{3}\,\mu} \overset{(27)}{=} \frac{\kappa\,R}{D\,\eta} \overset{(35)}{=} \frac{R}{D\,Z\,\gamma} \tag{39}$$

A.3 Two layers

A.3.1 Averaging

Defining coordinate z so that $z = 0$ corresponds to the interface between the two layers, the average of a function g over the two-layer structure is given by

$$\langle g \rangle := \frac{1}{L} \int_{-L_1}^{L_2} g(z)\,\mathrm{d}z = \frac{1}{L} \left(\int_{-L_1}^{0} g(z)\,\mathrm{d}z + \int_{0}^{L_2} g(z)\,\mathrm{d}z \right) \tag{40}$$

with $L := L_1 + L_2$.

A.3.2 Derivation of (A3-Norris)

Using (40), the averaged term in (38) is computed as follows:

$$\begin{aligned}
\langle \psi\, P_0 \rangle &= \frac{1}{L} \left(\int_{-L_1}^{0} \psi(z)\, P_0(z)\,\mathrm{d}z + \int_{0}^{L_2} \psi(z)\, P_0(z)\,\mathrm{d}z \right) \\
&= \frac{1}{L} \left(\int_{-L_1}^{0} \psi_1\, P_0(z)\,\mathrm{d}z + \int_{0}^{L_2} \psi_2\, P_0(z)\,\mathrm{d}z \right) \\
&= \frac{1}{L} \left(\psi_1 \underbrace{\int_{-L_1}^{0} P_0(z)\,\mathrm{d}z}_{:=I_1} + \psi_2 \underbrace{\int_{0}^{L_2} P_0(z)\,\mathrm{d}z}_{:=I_2} \right)
\end{aligned}$$

In the last equation, the first integral is

$$\begin{aligned}
I_1 &= \int_{-L_1}^{0} P_0(z)\,\mathrm{d}z \overset{(32)}{=} \\
&= \int_{-L_1}^{0} \left[A_1\, \cos(\gamma_1\, z) + B_1\, \sin(\gamma_1\, z) \right] \mathrm{d}z \\
&= A_1 \int_{-L_1}^{0} \cos(\gamma_1\, z)\,\mathrm{d}z + B_1 \int_{-L_1}^{0} \sin(\gamma_1\, z)\,\mathrm{d}z \\
&= \frac{A_1}{\gamma_1}\, \sin(\gamma_1\, L_1) - \frac{B_1}{\gamma_1} \left[1 - \cos(\gamma_1\, L_1) \right] \\
&= \frac{1}{\gamma_1} \left[A_1 \underbrace{\sin d_1}_{a_1} + B_1 \underbrace{(-1)\,(1-\cos d_1)}_{b_1} \right] \\
&= \frac{1}{\gamma_1} (A_1\, a_1 + B_1\, b_1)
\end{aligned} \tag{41}$$

where

$$a_1 := \sin d_1 \qquad b_1 := (-1)\,(1 - \cos d_1) \tag{42}$$

and the second integral is

$$\begin{aligned} I_2 &= \int_0^{L_2} P_0(z)\,\mathrm{d}z \overset{(32)}{=} \\ &= \int_0^{L_2} [A_2\,\cos(\gamma_2\,z) + B_2\,\sin(\gamma_2\,z)]\,\mathrm{d}z \\ &= A_2 \int_0^{L_2} \cos(\gamma_2\,z)\,\mathrm{d}z + B_2 \int_0^{L_2} \sin(\gamma_2\,z)\,\mathrm{d}z \\ &= \frac{A_2}{\gamma_2}\,\sin(\gamma_2\,L_2) + \frac{B_2}{\gamma_2}\,[1 - \cos(\gamma_2\,L_2)] \\ &= \frac{1}{\gamma_2}\,[A_2\,\underbrace{\sin d_2}_{a_2} + B_2\,(\underbrace{1 - \cos d_2}_{b_2})] \\ &= \frac{1}{\gamma_2}(A_2\,a_2 + B_2\,b_2) \end{aligned} \tag{43}$$

where

$$a_2 := \sin d_2 \qquad b_2 := 1 - \cos d_2 \tag{44}$$

so that

$$\begin{aligned} L\,\langle \psi\,P_0\rangle &= \psi_1\,I_1 + \psi_2\,I_2 \\ &= \sum_{j=1}^{2} \frac{\psi_j}{\gamma_j}(A_j\,a_j + B_j\,b_j) \\ &= \sum_{j=1}^{2} \frac{\psi_j}{\gamma_j}\,\left[A_j\,\sin d_j + (-1)^j\,B_j\,(1 - \cos d_j)\right] \end{aligned} \tag{45}$$

Thus (38) becomes

$$\frac{1}{p_{33}} = \frac{1}{c_{33}} - \frac{1}{L}\sum_{j=1}^{2} \frac{\psi_j}{\gamma_j}\,\left[A_j\,\sin d_j + (-1)^j\,B_j\,(1 - \cos d_j)\right] \tag{46}$$

whence we see that (46) is equivalent to (A3-Norris).

Morever, the coefficient ψ_j/γ_j in (46) may be written as

$$\frac{\psi_j}{\gamma_j} \overset{(39)}{=} \frac{R_j}{D_j\,Z_j\,\gamma_j^2} \overset{(30)}{=} \frac{1}{\mathrm{i}\,\omega}\,\frac{R_j}{Z_j} \tag{47}$$

and, therefore, (46) becomes

$$\frac{1}{p_{33}} = \frac{1}{c_{33}} - \frac{1}{\mathrm{i}\,\omega\,L}\sum_{j=1}^{2} \frac{R_j}{Z_j}\,\left[A_j\,\sin d_j + (-1)^j\,B_j\,(1 - \cos d_j)\right] \tag{48}$$

A.3.3 Derivation of (A4-Norris)

To determine parameters A_1, A_2, B_1, B_2, we use the following boundary conditions.
Periodicity:

$$P(z = -L_1) = P(z = L_2) \tag{49}$$

$$W(z = -L_1) = W(z = L_2) \tag{50}$$

Continuity:

$$P(z \uparrow 0^-) = P(z \downarrow 0^+) \tag{51}$$

$$W(z\uparrow 0^-) = W(z\downarrow 0^+) \tag{52}$$

With the stenographic notation

$$C_1 := \cos d_1 \qquad S_1 := \sin d_1 \qquad C_2 := \cos d_2 \qquad S_2 := \sin d_2 \tag{53}$$

equations (32) and (34) with conditions (49)–(52) yield

$$\begin{aligned} C_1\,A_1 - S_1\,B_1 + R_1 &= C_2\,A_2 + S_2\,B_2 + R_2 \\ -\frac{S_1}{Z_1}\,A_1 - \frac{C_1}{Z_1}\,B_1 &= \frac{S_2}{Z_2}\,A_2 - \frac{C_2}{Z_2}\,B_2 \\ A_1 + R_1 &= A_2 + R_2 \\ \frac{B_1}{Z_1} &= \frac{B_2}{Z_2} \end{aligned}$$

respectively. Solving these equations we get

$$\begin{pmatrix} A_1 \\ A_2 \\ B_1 \\ B_2 \end{pmatrix} = \frac{R_1 - R_2}{Z_1\cot(d_1/2) + Z_2\cot(d_2/2)} \begin{pmatrix} -Z_1\cot(d_1/2) \\ Z_2\cot(d_2/2) \\ Z_1 \\ Z_2 \end{pmatrix}$$

which, substituted into (48), yields (A4-Norris).

Moreover, using the stenographic notation (53), eqs. (42) and (44) become

$$a_1 = S_1 \qquad a_2 = S_2 \qquad b_1 = C_1 - 1 \qquad b_2 = 1 - C_2 \tag{54}$$

A.4 Generalization of Appendix A of Norris: three layers

A.4.1 Averaging

Defining coordinate z so that $z = 0$ corresponds to the interface between layer 1 and layer 2, the average of a function g over the three-layer structure is given by

$$\begin{aligned} \langle g\rangle &:= \frac{1}{L}\int_{-L_1}^{L_2+L_3} g(z)\,\mathrm{d}z \\ &= \frac{1}{L}\left(\int_{-L_1}^{0} g(z)\,\mathrm{d}z + \int_{0}^{L_2} g(z)\,\mathrm{d}z + \int_{L_2}^{L_2+L_3} g(z)\,\mathrm{d}z\right) \end{aligned} \tag{55}$$

where $L := L_1 + L_2 + L_3$, with L_j the thickness of layer j.

A.4.2 Generalization of (A3-Norris)

Using (55), the averaged term in (38) is computed as follows:

$$\begin{aligned} L\,\langle\psi\,P_0\rangle &= \int_{-L_1}^{0}\psi(z)\,P_0(z)\,\mathrm{d}z + \int_{0}^{L_2}\psi(z)\,P_0(z)\,\mathrm{d}z + \int_{L_2}^{L_2+L_3}\psi(z)\,P_0(z)\,\mathrm{d}z \\ &= \int_{-L_1}^{0}\psi_1\,P_0(z)\,\mathrm{d}z + \int_{0}^{L_2}\psi_2\,P_0(z)\,\mathrm{d}z + \int_{L_2}^{L_2+L_3}\psi_3\,P_0(z)\,\mathrm{d}z \\ &= \psi_1\underbrace{\int_{-L_1}^{0}P_0(z)\,\mathrm{d}z}_{:=I_1} + \psi_2\underbrace{\int_{0}^{L_2}P_0(z)\,\mathrm{d}z}_{:=I_2} + \psi_3\underbrace{\int_{L_2}^{L_2+L_3}P_0(z)\,\mathrm{d}z}_{:=I_3} \\ &= \sum_{j=1}^{3}\psi_j\,I_j \end{aligned} \tag{56}$$

In the last equation, the first integral is given by equation (41), and the second integral is given by equation (43). Likewise, the third integral yields

$$
\begin{aligned}
I_3 &:= \int_{L_2}^{L_2+L_3} P_0(z)\,\mathrm{d}z \\
&\overset{(32)}{=} \int_{L_2}^{L_2+L_3} [A_3\,\cos(\gamma_3\,z) + B_3\,\sin(\gamma_3\,z)]\,\mathrm{d}z \\
&= A_3 \int_{L_2}^{L_2+L_3} \cos(\gamma_3\,z)\,\mathrm{d}z + B_3 \int_{L_2}^{L_2+L_3} \sin(\gamma_3\,z)\,\mathrm{d}z \\
&= \frac{A_3}{\gamma_3}\,\big[\sin(\gamma_3\,z)\big]_{z=L_2}^{z=L_2+L_3} + \frac{B_3}{\gamma_3}\,\big[-\cos(\gamma_3\,z)\big]_{z=L_2}^{z=L_2+L_3} \\
&= \frac{A_3}{\gamma_3}\,\big\{\sin[\gamma_3\,(L_2+L_3)] - \sin(\gamma_3\,L_2)\big\} - \frac{B_3}{\gamma_3}\,\big\{\cos[\gamma_3\,(L_2+L_3)] - \cos(\gamma_3\,L_2)\big\} \\
&= \frac{1}{\gamma_3}\,\{A_3\,\big[\sin(\gamma_3\,L_2+\gamma_3\,L_3) - \sin(\gamma_3\,L_2)\big] - B_3\,\big[\cos(\gamma_3\,L_2+\gamma_3\,L_3) - \cos(\gamma_3\,L_2)\big]\} \\
&= \frac{1}{\gamma_3}\,\{A_3\,\underbrace{\big[\sin\left(d_3\,\frac{L_2}{L_3}+d_3\right) - \sin\left(d_3\,\frac{L_2}{L_3}\right)\big]}_{a_3} + B_3\,\underbrace{(-1)\,\big[\cos\left(d_3\,\frac{L_2}{L_3}+d_3\right) - \cos\left(d_3\,\frac{L_2}{L_3}\right)\big]}_{b_3}\} \\
&= \frac{1}{\gamma_3}\,(A_3\,a_3 + B_3\,b_3)
\end{aligned}
\tag{57}
$$

where

$$
\begin{aligned}
a_3 &:= C_{23}\,S_3 - S_{23}\,(1-C_3) \\
b_3 &:= S_{23}\,S_3 + C_{23}\,(1-C_3)
\end{aligned}
\tag{58}
$$

with

$$
C_3 := \cos(d_3) \qquad S_3 := \sin(d_3) \qquad C_{23} := \cos\left(\frac{L_2}{L_3}\,d_3\right) \qquad S_{23} := \sin\left(\frac{L_2}{L_3}\,d_3\right) \tag{59}
$$

Therefore

$$
\begin{aligned}
L\,\langle\psi\,P_0\rangle &\overset{(56)}{=} \sum_{j=1}^{3} \psi_j\,I_j \\
&\overset{(41),\,(43),\,(57)}{=} \sum_{j=1}^{3} \frac{\psi_j}{\gamma_j}\,(A_j\,a_j + B_j\,b_j)
\end{aligned}
$$

Thus (38) becomes

$$
\begin{aligned}
\frac{1}{p_{33}} &= \frac{1}{c_{33}} - \langle\psi\,P_0\rangle \\
&= \frac{1}{c_{33}} - \frac{1}{L}\,\sum_{j=1}^{3} \frac{\psi_j}{\gamma_j}\,(A_j\,a_j + B_j\,b_j)
\end{aligned}
\tag{60}
$$

which is a three-layer generalization of (A3-Norris).

Using (47), equation (60) may be written as

$$
\frac{1}{p_{33}} = \frac{1}{c_{33}} - \frac{1}{\mathrm{i}\,\omega\,L}\,\sum_{j=1}^{3} \frac{R_j}{Z_j}\,(A_j\,a_j + B_j\,b_j) \tag{61}
$$

which generalizes (A3-Norris).

A.5 Generalization of (A4-Norris)

To determine the six parameters A_j, B_j (with $j = 1, 2, 3$) we use the following six boundary conditions:

$$\text{periodicity} \begin{cases} P(z = -L_1) = P(z = L_2 + L_3) \\ W(z = -L_1) = W(z = L_2 + L_3) \end{cases} \tag{62}$$

$$\text{continuity} \begin{cases} P(z \uparrow 0^-) = P(z \downarrow 0^+) \\ W(z \uparrow 0^-) = W(z \downarrow 0^+) \\ P(z \uparrow L_2^-) = P(z \downarrow L_2^+) \\ W(z \uparrow L_2^-) = W(z \downarrow L_2^+) \end{cases} \tag{63}$$

Equations (32) and (34) with conditions (62)–(63) yield

$$\begin{aligned} A_1\,C_1 - B_1\,S_1 + R_1 &= A_3\;(C_3\,C_{23} - S_3\,S_{23}) + B_3\;(C_{23}\,S_3 + C_3\,S_{23}) + R_3 \\ -\frac{1}{Z_1}\;(A_1\,S_1 + B_1\,C_1) &= \frac{1}{Z_3}[A_3\;(C_{23}\,S_3 + C_3\,S_{23}) + B_3\;(S_3\,S_{23} - C_3\,C_{23})] \\ A_1 + R_1 &= A_2 + R_2 \\ \frac{B_1}{Z_1} &= \frac{B_2}{Z_2} \\ A_2\,C_2 + B_2\,S_2 + R_2 &= A_3\,C_{23} + B_3\,S_{23} + R_3 \\ \frac{1}{Z_2}\,(A_2\,S_2 - B_2\,C_2) &= \frac{1}{Z_3}\,(A_3\,S_{23} - B_3\,C_{23}) \end{aligned} \tag{64}$$

Finally, equations (64) are solved, through straightforward computations, to obtain A_j, B_j for $j = 1, 2, 3$. As these symbolic expressions are somewhat cumbersome, they are omitted here for brevity. Substituting the values of A_j, B_j so obtained, together with (54) and (58), into eq. (61), one obtains a generalization of (A4-Norris).

Table 1. Material properties

Grain	bulk modulus, K_s	33.4 GPa
	shear modulus, μ_s	30 GPa
	density, ρ_s	2650 kg/m^3
Frame	bulk modulus, K_m	1.3 GPa
	shear modulus, μ_m	1.4 GPa
	porosity, ϕ	0.3
	permeability, κ	1 darcy
Brine	density, ρ_B	975 kg/m^3
	viscosity, η_B	0.001 Pa s
	bulk modulus, K_B	2.2 GPa
Oil	density, ρ_o	870 kg/m^3
	viscosity, η_o	0.3 Pa s
	bulk modulus, K_o	2 GPa
Gas	density, ρ_g	70 kg/m^3
	viscosity, η_g	0.00015 Pa s
	bulk modulus, K_g	0.0096 GPa

1 darcy = 9.869233×10^{-13} m^2

Table 2. Saturations. Homogeneous frame (L = 60 cm).

Case	S_b (%)	S_o (%)	S_g (%)
1	100/3	100/3	100/3
2	60	20	20
3	20	60	20
4	20	20	60
5	49.5	49.5	1

b: brine; o: oil; g: gas

Table 3. Heterogeneous frame (L = 60 cm). (oil saturated)

Case	L_1 (cm)	L_2 (cm)	L_3 (cm)
1	20	20	20
2	36	12	12
3	12	36	12
4	12	12	36
5	0.6	29.7	29.7
ϕ (%)	30	20	10
K_m (GPa)	7.2	14.5	23.5
μ_m (GPa)	6.5	13	21.1
κ (darcy)	1	0.24	0.02

1 darcy = 9.869233×10^{-13} m^2

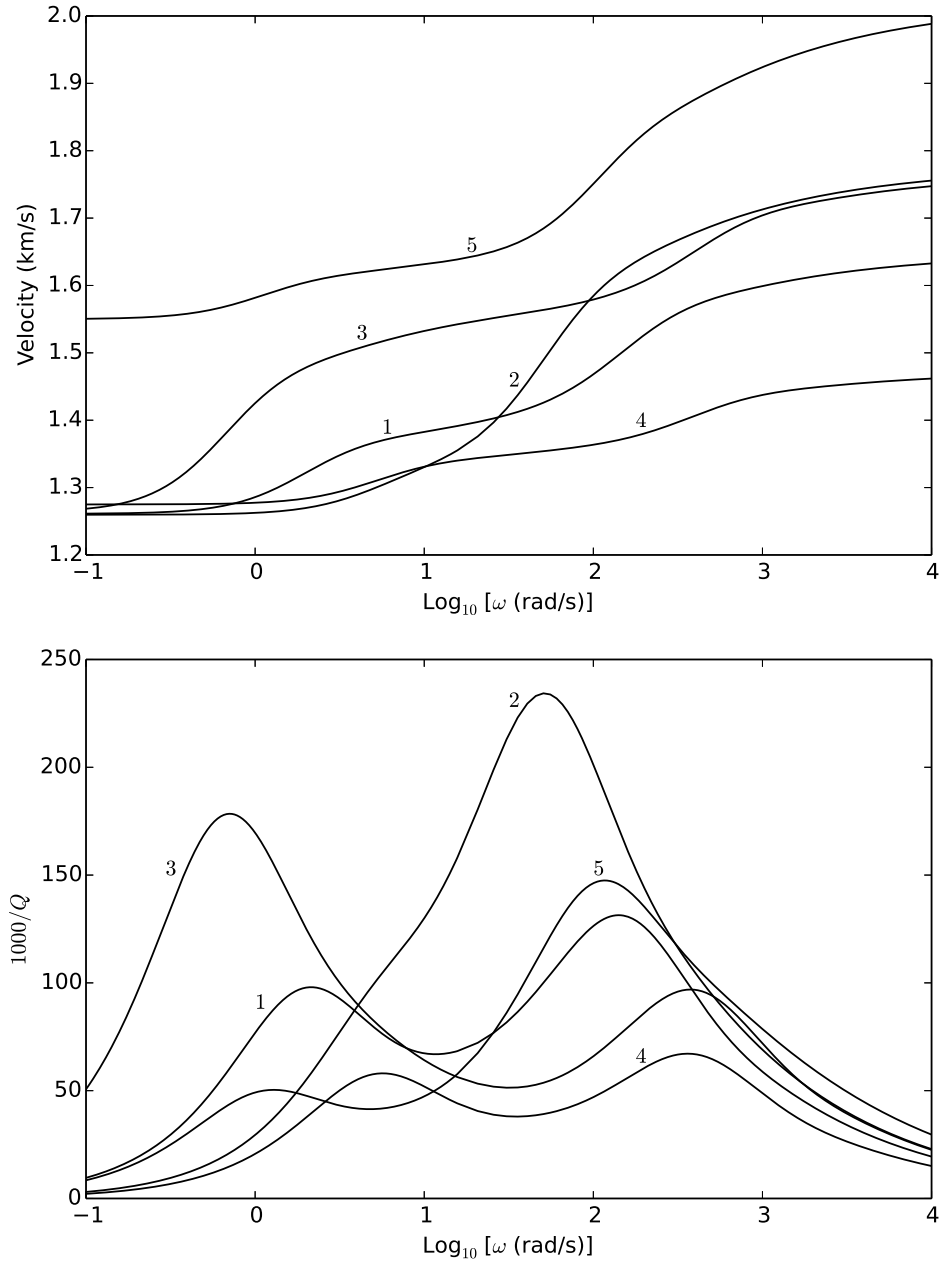

Fig. 1 P-wave phase velocity (a) and dissipation factor (b) corresponding to the cases shown in Table 2.

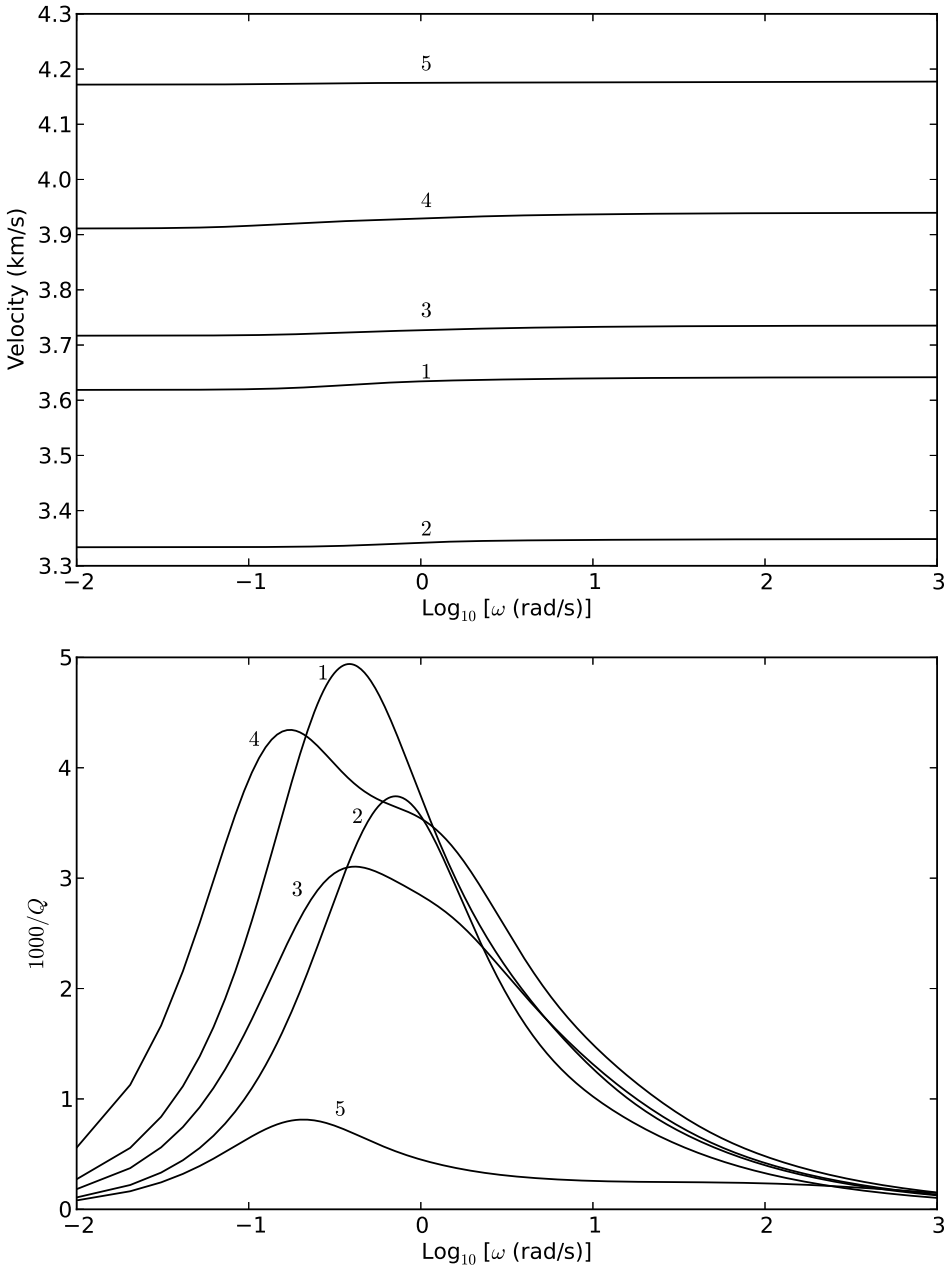

Fig. 2 P-wave phase velocity (a) and dissipation factor (b) corresponding to the cases shown in Table 3. These properties correspond to the direction perpendicular to the layering plane.

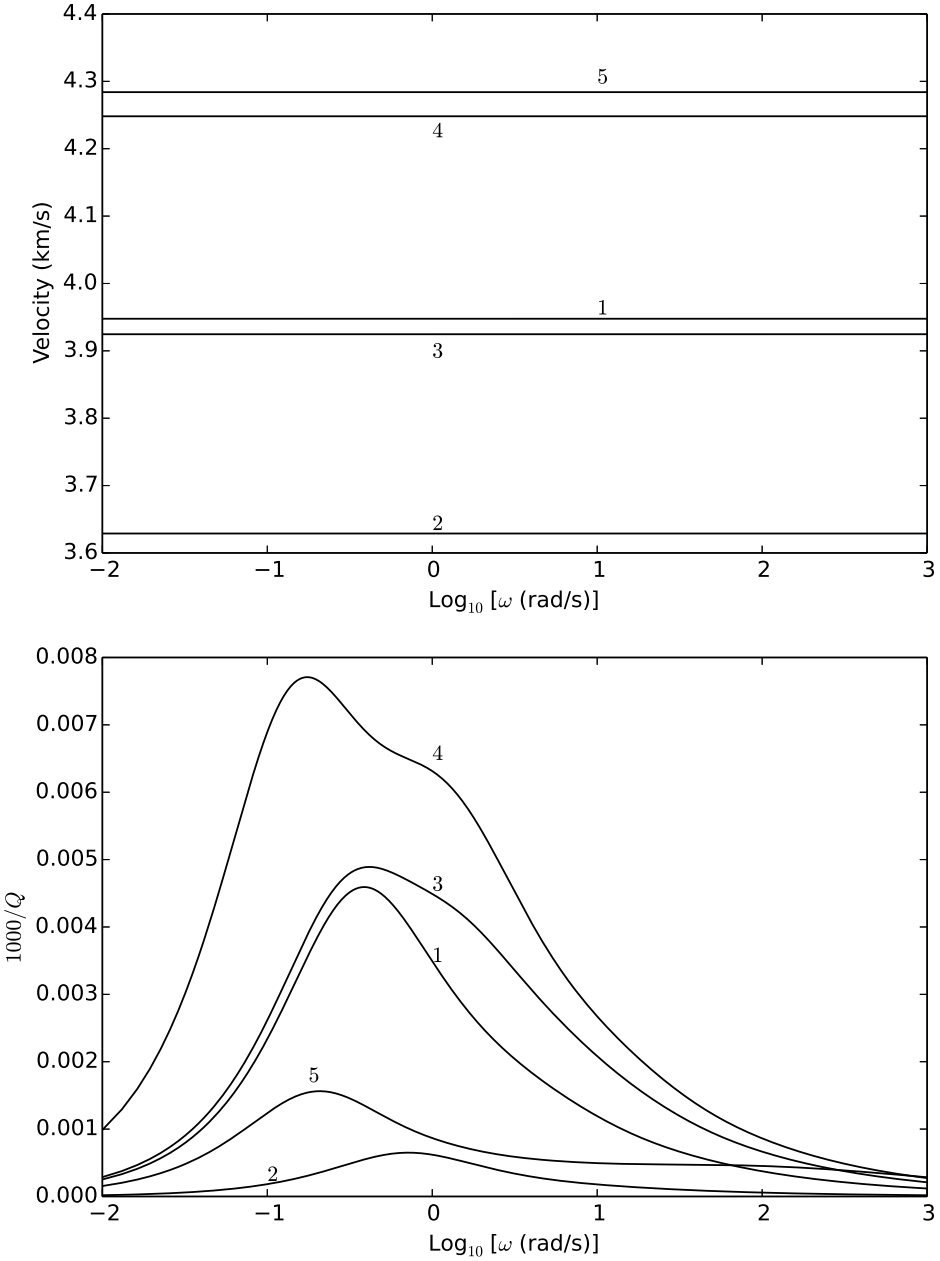

Fig. 3 P-wave phase velocity (a) and dissipation factor (b) corresponding to the cases shown in Table 3. These properties correspond to the direction parallel to the layering plane.

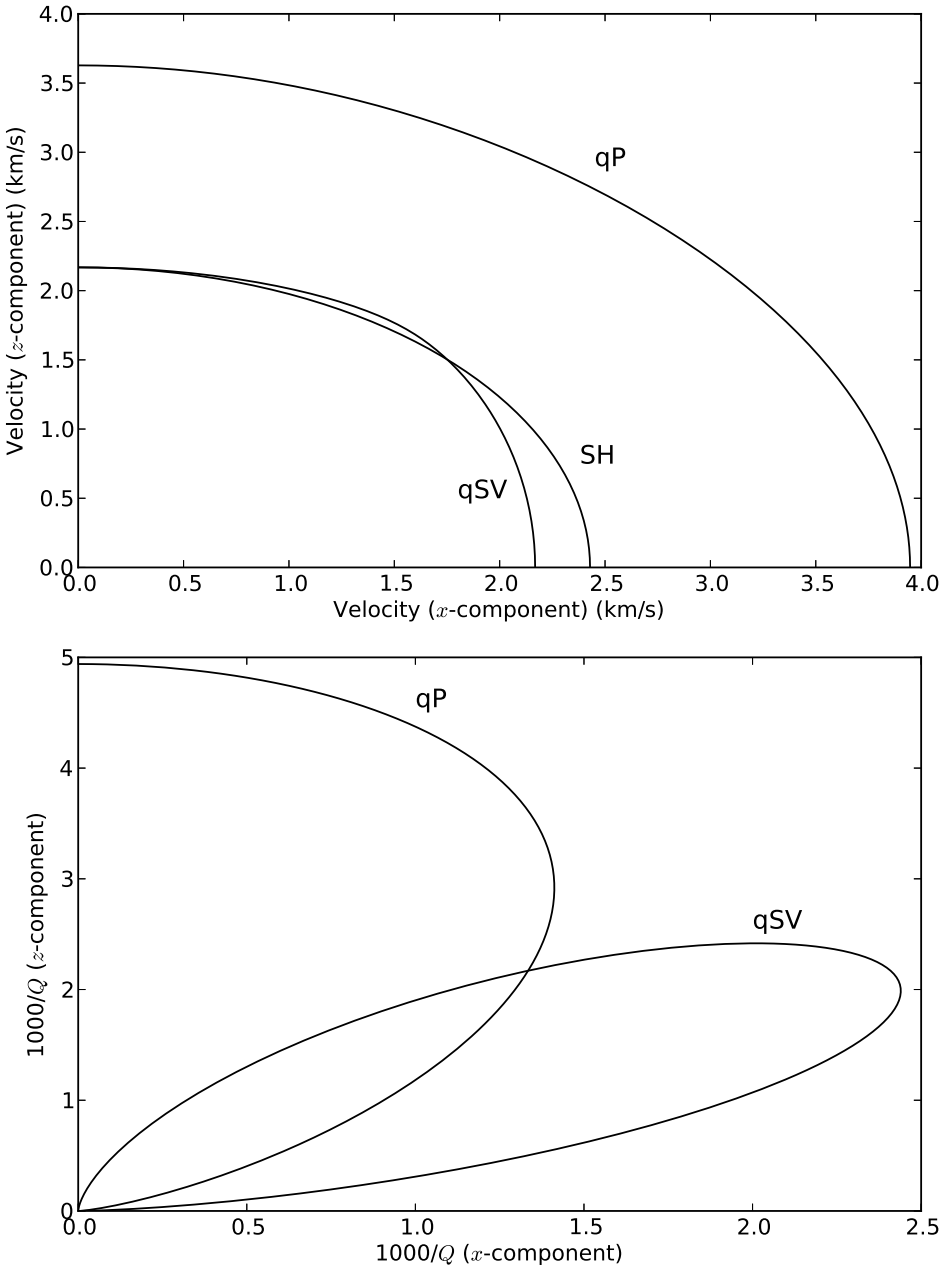

Fig. 4 Polar representation of the energy velocity (a) and dissipation factor (b) corresponding to Case 1 shown in Table 3 at a frequency of 0.06 Hz.

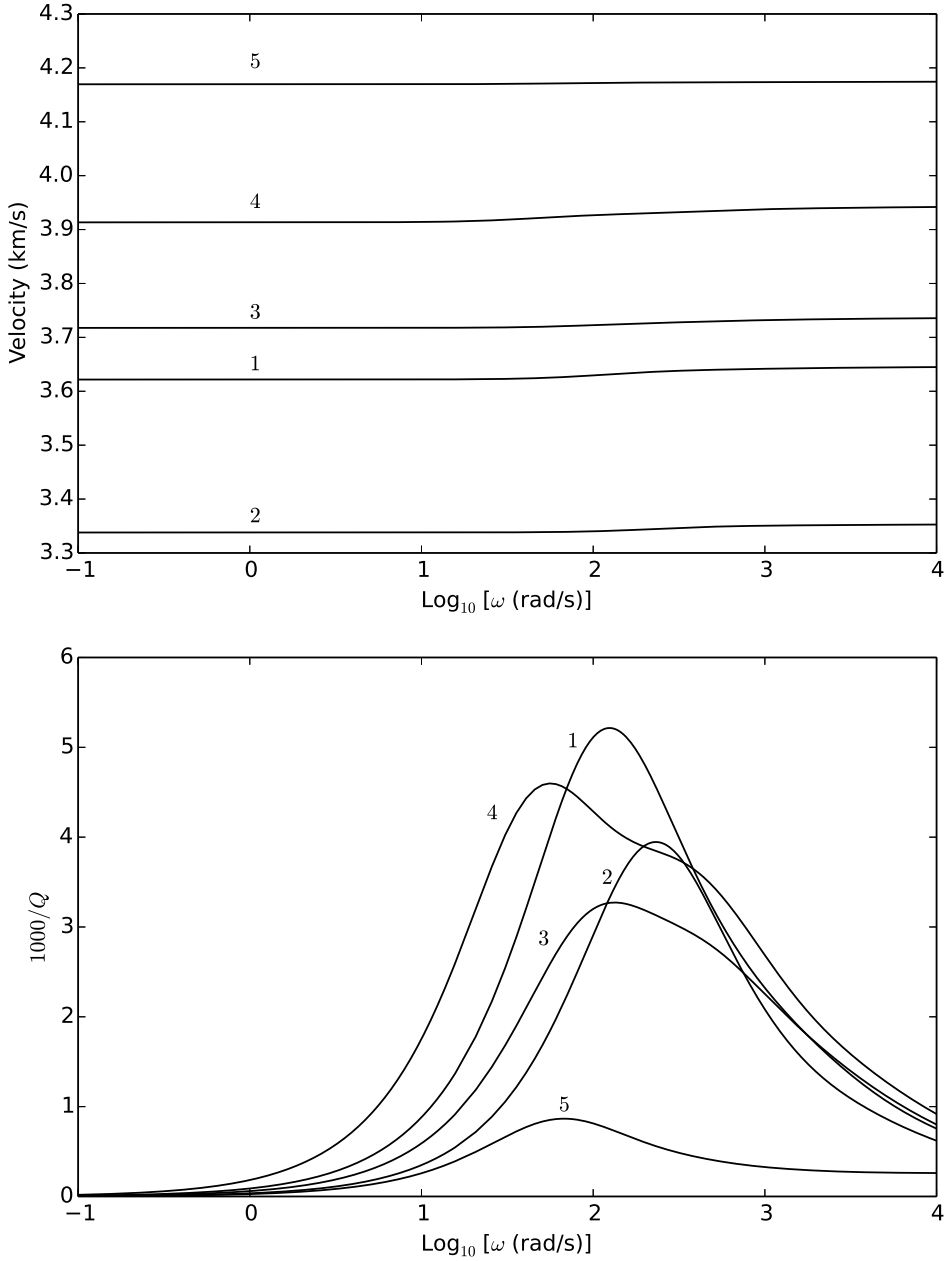

Fig. 5 Phase velocity (a) and dissipation factor (b) corresponding to the cases shown in Table 3, where oil has been replaced by brine. These properties correspond to the direction perpendicular to the layering plane.

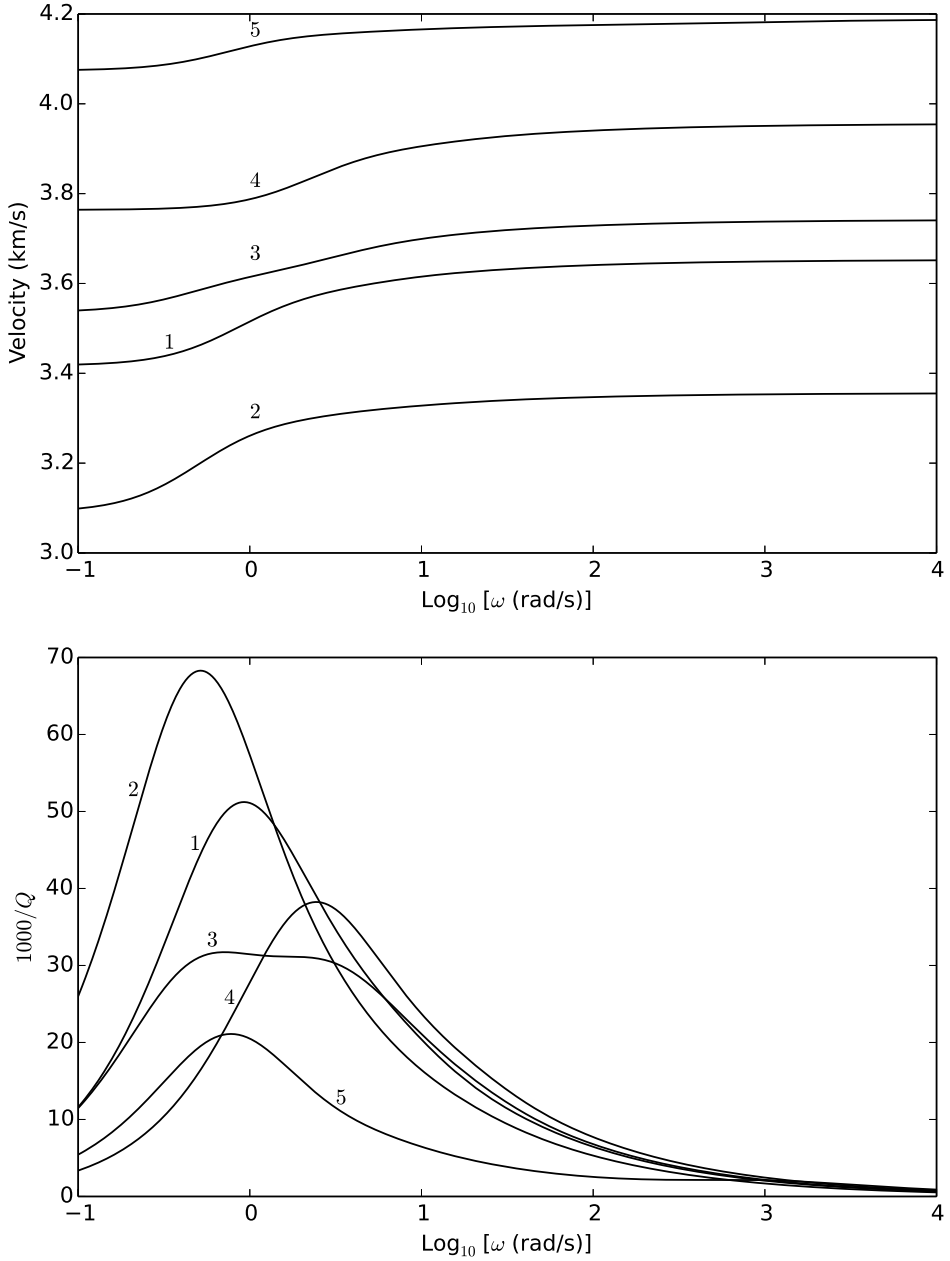

Fig. 6 Phase velocity (a) and dissipation factor (b) corresponding to the cases shown in Table 3, where layers 1 and 2 are saturated with oil and the third layer is saturated with gas. These properties correspond to the direction perpendicular to the layering plane.

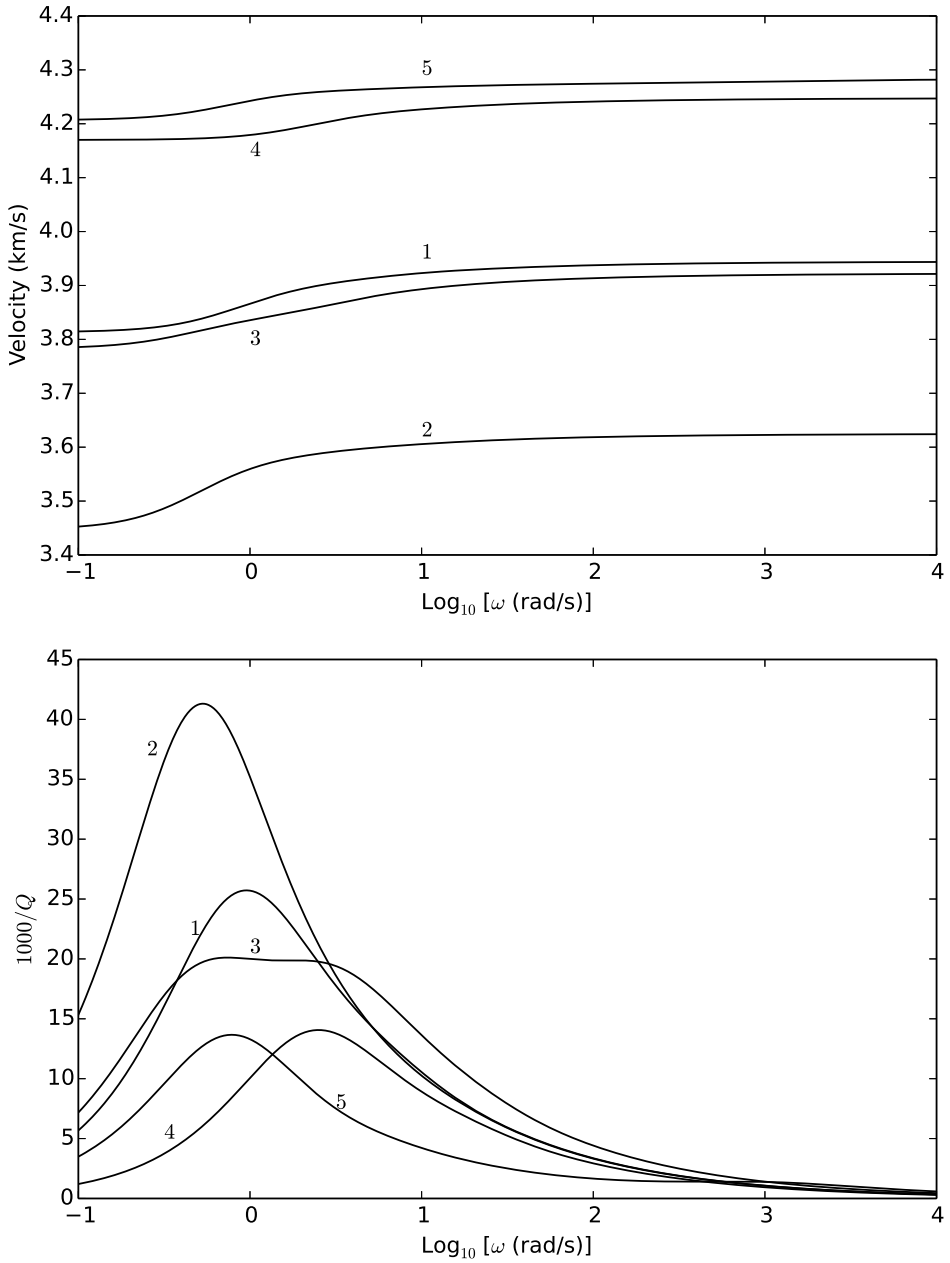

Fig. 7 Phase velocity (a) and dissipation factor (b) corresponding to the cases shown in Table 3, where layers 1 and 2 are saturated with oil and the third layer is saturated with gas. These properties correspond to the direction parallel to the layering plane.